Determination of Molecular Geometry in Solid-State NMR: Rotational-Echo Double Resonance of Three-Spin Systems

Frederick G. Vogt,*,† James M. Gibson,‡ Sue M. Mattingly, and Karl T. Mueller*

Department of Chemistry, The Pennsylvania State University, 152 Davey Laboratory, University Park, Pennsylvania 16802

Received: July 22, 2002; In Final Form: November 12, 2002

The precise measurement of internuclear distances in solids by NMR has been widely explored using experiments that measure the dipolar coupling between labeled spin pairs. The rotational-echo double-resonance (REDOR) experiment is one of the most successful techniques for quantifying distances between heteronuclei. In the present work, REDOR is applied to the precise determination of the angle between internuclear vectors in triply labeled spin systems. The time domain REDOR signal for two heteronuclear coupled spin pairs sharing a common partner (an I_2S spin system) is derived and analyzed with the aid of dipolar transforms. A two-step experimental approach for the structural analysis of I_2S spin systems is then developed. Independent θ-REDOR and traditional REDOR measurements are used to obtain the heteronuclear dipolar coupling constants and the angle between them. Demonstrations are carried out on labeled polycrystalline samples of glycine and uracil. The REDOR experiment is also examined using alternate nuclei in the three-spin system as the detection point, as a supplement to the θ-REDOR technique. The precision of the experimental angular determinations for glycine and uracil was calculated by the method of Cramér-Rao lower bounds and was found to be greater than in previous REDOR-based analyses. The approach demonstrated here is not limited to crystalline materials and may be employed for structural measurements in systems in which X-ray crystallographic studies are not feasible.

I. Introduction

Solid-state NMR can be used to determine the distance between nuclear spins by measurement of the through-space magnetic dipolar coupling. The magnitude of the dipolar coupling exhibits an inverse cubic dependence on the internuclear distance and is often relatively weak in cases of interest. Techniques have therefore been developed for dipolar coupling measurements in the presence of other overwhelming interactions, such as chemical-shift anisotropy and stronger dipolar couplings. One common strategy involves the suppression of stronger interactions using magic-angle spinning[1−3] (MAS) and heteronuclear dipolar decoupling of protons,[3] often in conjunction with the sensitivity-enhancing cross-polarization (CP) technique.[3−5] The dipolar interaction of interest is then selectively reintroduced by radio frequency (RF) pulse sequences and measured under high-resolution conditions. One of the most successful methods of this type is the rotational-echo double-resonance (REDOR) experiment, which is primarily used for the measurement of weak heteronuclear couplings between spin-$^1/_2$ nuclei.[6−9] Several versions of the REDOR experiment have been employed for the measurement of dipolar couplings in many different systems, including $^{13}C-^{15}N$, $^{13}C-^{19}F$, and $^{13}C-^{31}P$ spin pairs in biologically relevant molecules.[10−19] Other recent applications have measured $^{6}Li-^{13}C$ distances in organometallic compounds,[20] $^{2}H-^{13}C$ distances in polymers,[21] and $^{19}F-^{29}Si$ distances in microcrystalline molecular sieve systems.[22] In many cases, REDOR experiments have provided structural information that would have been difficult or impossible to obtain with other techniques.

Isotopic labeling is commonly used to prepare samples for a REDOR study to ensure a simplified dipolar interaction between two isolated heteronuclear spins I and S (Figure 1a). In these cases, or when naturally occurring abundant spin pairs are available, the dipolar coupling and the internuclear distance r can be readily extracted from the REDOR time domain signal.[6−8] In more complicated situations, such as several isolated spin pairs with different internuclear distances, more sophisticated data processing techniques are helpful. A dipolar spectrum can be generated using the REDOR transform (or other related techniques) that will theoretically contain a peak for each dipolar coupling in the system.[23,24] The dipolar spectrum is generally superior to the broad powder spectra obtained from the Fourier transform (FT), which have poor signal-to-noise ratios and overlapping features.[7,23−25] The REDOR transform simplifies the analysis of multiple dipolar couplings and distributions of couplings and has been applied to the measurement of multiple internuclear distances in a single experiment.[26] However, the REDOR transform does not allow for the direct extraction of distance information from spin triads or more complicated spin clusters, since these situations involve the relative orientations and magnitudes of more than one dipolar interaction.

Angular measurements by high-resolution solid-state NMR, including torsional angle determinations, have also been the subject of recent research efforts.[27−33] Most studies determine the relative orientation of chemical shift interactions through dipolar-mediated interference effects. The REDOR experiment has also been used in this manner to study the relative orientations of dipolar and chemical shift tensors, as the principal

* Corresponding authors.
† Present address: Chemical Development, GlaxoSmithKline P.L.C., 709 Swedeland Rd., P. O. Box 1539, King of Prussia, PA, 19406.
‡ Present address: Department of Bioengineering, University of Washington, Seattle, WA, 98195-1700.

10.1021/jp021686f CCC: $25.00
Published on Web 01/10/2003

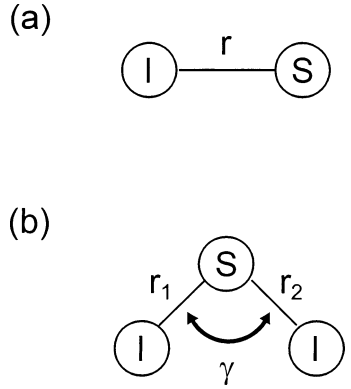

Figure 1. Spin systems examined in this work. In (a), a *S*-spin interacts with an *I*-spin through a heteronuclear dipolar coupling over an internuclear distance *r*. The I_2S spin system is shown in (b). Its geometry is specified by two internuclear distances (r_1 and r_2) and an angle (γ).

axis system (PAS) of the dipolar interaction is easily assigned to the internuclear vector.[34] Interference effects between multiple dipolar interactions, without the use of a chemical shift interaction, represent another avenue toward angular measurements. Effects of this sort have been known for some time, particularly those involving the homonuclear dipolar interaction.[35] Heteronuclear dipolar interference is detectable in REDOR studies of several *I* spins coupled to a single *S* spin (with the *S* spin being experimentally detected). Published work on I_nS systems has examined the complicating effect of extraneous natural abundance spins on *IS* REDOR distance measurements, and additional averaging effects of molecular motion.[36−38] Actual REDOR measurements of the angle between two dipolar interactions have only appeared recently and have been focused on the simplest and most promising I_2S system (depicted in Figure 1b), where the angle between the two heteronuclear dipolar interactions is denoted by γ. For example, an in-depth REDOR study of an I_2S system and its potential geometrical information was recently published, in which γ values in labeled peptides were determined to a moderate precision (from ±4° to ±9°) by numerical analysis of the time domain REDOR signal.[39] A second study also investigated aspects of this problem and indicated that the angle is difficult to determine precisely.[40] Work has also focused on characterizing the short-time behavior of REDOR signals from I_2S systems, avoiding geometry issues by using a second moment analysis.[41]

To study the geometry of an I_2S spin triad, it is desirable to separately measure the two distances r_1 and r_2 without observing their mutual interference. Substantial progress has been made in achieving "spin-pair" distance measurements in I_2S systems with specialized pulse sequences, including θ-REDOR, FDR−REDOR, DANTE-selected REDOR, and other techniques.[42−46] These advances have made it possible to efficiently measure *IS* distances in I_2S triads. The interference of the heteronuclear dipolar interactions can then be detected in a traditional REDOR experiment and used to determine γ via a single-variable nonlinear fitting procedure. The fit can be accomplished directly on the time domain I_2S REDOR signal. The signal can also be processed with techniques designed to avoid the range of dipolar frequencies present in REDOR signals, which cause it to decay quickly and make spectral analysis less reliable.[25] For example, the signal can be analyzed by the REDOR transform to produce a dipolar interference pattern with refined features. Although the dipolar spectrum is not directly interpreted to obtain internuclear distances in the usual manner, the structured line shape can be used to both identify the presence of an I_2S system and to precisely fit the angle γ.

In the present work, a detailed analysis is made of the REDOR experiment as applied to the I_2S spin system. The features of the *S*-detected REDOR signal are shown to be strongly dependent on the angle between the heteronuclear dipolar interactions, while the signal detected on the *I*-spin has no dependence on γ (unless additional interactions are present). Independent 2D triple-resonance θ-REDOR experiments[44] and *S*-detected REDOR experiments are used to determine the internuclear distances r_1 and r_2 and the angle γ in two simple molecules (containing isolated $^{13}C/^{15}N$ triads) that have been characterized by X-ray crystallography. For the experimental cases studied here, the angular determination is found to be considerably more precise than previously reported.[39,40] Applications of REDOR transform analysis to I_2S REDOR signals are also explored and are found to be useful for detection of dipolar interference and measurement of γ via nonlinear fitting. The methods presented here are intended for more interesting and complicated situations where diffraction techniques may not be applicable. Although the required spin system is unlikely to occur in nature, synthetic spin labeling can be employed (as in many REDOR studies) to insert I_2S systems into molecules of interest.[10−19]

II. Theoretical Background

Dipolar Evolution Under REDOR in I_2S Systems. For clarity, a heteronuclear, dipolar-coupled pair of spin-$^1/_2$ nuclei (denoted by *I* and *S*) is considered first. The spins are assumed to be isolated so that other dipolar interactions are insignificant. The total Hamiltonian for this system is

$$\mathscr{H} = \mathscr{H}_D^{IS} + \mathscr{H}_{CS}^{I} + \mathscr{H}_{CS}^{S} + \mathscr{H}_J^{IS} \quad (1)$$

The individual Hamiltonians in eq 1 commute with each other at all times, and represent the heteronuclear dipolar interaction between the spins, the individual anisotropic chemical shift interactions, and a possible isotropic heteronuclear *J*-coupling interaction. Magic-angle spinning imparts a time-dependence to local dipolar magnetic fields and the chemical shift anisotropy.[3,47] Under this mechanical motion the heteronuclear dipolar Hamiltonian for the spin pair is[3]

$$\mathscr{H}_D^{IS}(\alpha,\beta,t) = \omega_D(\alpha,\beta,t) I_z S_z \quad (2)$$

$$\omega_D(\alpha,\beta,t) = \pm\pi D_{IS}[\sin^2\beta\cos 2(\alpha + 2\pi\nu_r t) - \sqrt{2}\sin(2\beta)\cos(\alpha + 2\pi\nu_r t)] \quad (3)$$

where ω_D is the time-dependent dipolar frequency under MAS, I_z and S_z are the spin angular momentum operators, α and β are the azimuthal and polar powder angles describing the orientation of the heteronuclear dipolar vector in the frame defined by the MAS rotor, and ν_r is the rotor speed in Hz. Equations 2 and 3 are scaled by D_{IS}, the time-independent dipolar coupling between the *I* and *S*-spins:

$$D_{IS} = \frac{\gamma_I \gamma_S \hbar \mu_0}{8\pi^2 r_{IS}^3} \quad (4)$$

Here γ_I and γ_S are the gyromagnetic ratios of the spins, $\hbar$ is Planck's constant divided by 2π, μ_0 is the free space permeability, and r_{IS} is the internuclear distance between the spins. The relationship between D_{IS} and r_{IS} in eq 4 provides

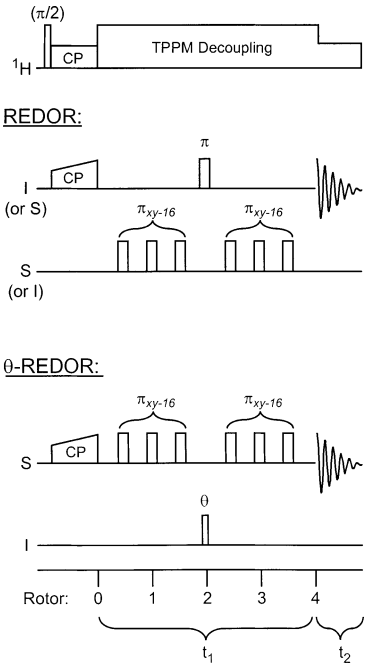

Figure 2. The 2D-REDOR pulse sequences used in this work. At the top, the traditional triple-resonance REDOR pulse sequence is depicted. It can be used to measure both distances and angles in I_2S systems, via *I* and *S*-detected versions. At the bottom is shown the θ-REDOR pulse sequence, which creates a "spin-pair" signal in multiple spin systems and is always performed as an *S*-detected experiment. The θ-pulse used here had a flip angle of 40°.

the motivation for distance measurements via dipolar couplings. Equations 2−4 indicate that the effects of the heteronuclear dipolar interaction will average to zero if the rotor period is short relative to the inverse magnitude of the dipolar coupling. The chemical shift interaction averages to its isotropic value in a similar manner, as do weaker, isolated homonuclear dipolar interactions, although the isotropic heteronuclear *J*-coupling remains.[47]

In the 2D-REDOR experiment, the second dimension is used to observe evolution under the Hamiltonian in eq 2. The 2D-REDOR sequences used here (Figure 2) reintroduce the heteronuclear dipolar interaction by periodically inverting its sign with π pulses every half-rotor period (following a preparatory cross-polarization sequence). The second dimension is sampled stroboscopically at a time t_1, which is an even integral multiple of the rotor period (i.e., $t_1 = N\tau_r$, where $\tau_r = 1/\nu_r$). The evolution in the t_1 dimension is governed by a cyclic, rotor-synchronized pulse sequence; thus, the observed signal can be found from a zeroth-order average Hamiltonian:

$$\bar{\mathscr{H}}_D^{IS}(\alpha,\beta,t_1) = \frac{1}{t_1}\int_0^{t_1} \mathscr{H}_D^{IS}(t')\,dt' = \Delta\phi_D(\alpha,\beta,t_1) I_z S_z \quad (5)$$

The time-dependence of the Hamiltonian in eq 2 is removed by integration over t_1. Since a single rotor period represents the basic "building block" of the sequence, the integration amounts to a calculation of the phase $\Delta\phi_D$ accumulated by a crystallite experiencing π pulses at the middle and the end of the rotor period: [6−8]

$$\Delta\phi_D(\alpha,\beta,t_1) = N\left(\int_0^{\tau_r/2}\omega_D(\alpha,\beta,t)\,dt - \int_{\tau_r/2}^{\tau_r}\omega_D(\alpha,\beta,t)\,dt\right) = \pm 4\sqrt{2} D_{IS} t_1 [\sin\beta\cos\beta\sin\alpha] \quad (6)$$

This phase would be zero at $t_1 = N\tau_r$ in a normal MAS experiment. In REDOR, the presence of the RF pulses leads to dephasing as a function of t_1 and D_{IS}. The dipolar dephasing signal can be obtained from the integrated Liouville-von Neumann equation for the density matrix $\rho(t_1)$:

$$\rho(t_1) = e^{-i\bar{\mathscr{H}}_D^{IS} t_1}\rho(0)\, e^{i\bar{\mathscr{H}}_D^{IS} t_1} \quad (7)$$

where the initial density matrix $\rho(0)$ is a coherent state prepared by the CP sequence. The implicit constraint on t_1, linking it to the period of the Hamiltonian, now ensures that the signal will be sampled at a dipolar rotational echo. Only the heteronuclear dipolar Hamiltonian is shown in eq 7, because the pulse(s) on the detected spin cause spin−echoes that refocus the chemical shift interaction at the start of acquisition, removing its effects from the REDOR t_1 dimension. In addition, the pulse sequences discussed here also eliminate the effects of any heteronuclear isotropic scalar interaction in the t_1 dimension.[48]

The situation for a three-spin system of the form I_2S is more complicated. Both heteronuclear dipolar interactions and a possible homonuclear *J*-coupling between the *I*-spins must be taken into account:

$$\mathscr{H}^{I_2S}(t) = \omega_D^{(1)}(\alpha^{(1)},\beta^{(1)},t) I_z^{(1)} S_z + \omega_D^{(2)}(\alpha^{(2)},\beta^{(2)},t) I_z^{(2)} S_z + \omega_J^{II} I_z^{(1)} I_z^{(2)} \quad (8)$$

where the *J*-coupling is assumed to be weak and the dipolar frequency of each of the two anisotropic *IS* couplings ($i = 1$, 2) depends on its individual orientation:

$$\omega_D^{(i)}(\alpha^{(i)},\beta^{(i)},t) = \pm\pi D_{IS}^{(i)} [\sin^2\beta^{(i)}\cos 2(\alpha^{(i)} + 2\pi\nu_r t) - \sqrt{2}\sin(2\beta^{(i)})\cos(\alpha^{(i)} + 2\pi\nu_r t)] \quad (9)$$

The homonuclear isotropic *J*-interaction between the *I*-spins, which is not refocused by the REDOR experiments discussed here,[49] is characterized by the constant ω_J^{II} (the *J*-coupling in rad/sec). It is assumed that the MAS rate is rapid enough to remove any homonuclear dipolar couplings between the *I*-spins, and that the chosen REDOR pulse sequence will not reintroduce this interaction through SEDRA or RFDR-type effects.[9,50] The expression analogous to eq 6 is then

$$\Delta\phi_D^{(i)}(\alpha^{(i)},\beta^{(i)},t_1) = \pm 4\sqrt{2} D_{IS}^{(i)} t_1 [\sin\beta^{(i)}\cos\beta^{(i)}\sin\alpha^{(i)}] \quad (10)$$

because of the fact that the two individual heteronuclear dipolar interactions commute. An average Hamiltonian like that of eq 5 can then be written.

Since the principal axis systems of the dipolar interactions are unlikely to coincide, real-space interference effects can occur if coherence can be transferred in spin-space via the active Hamiltonians. Whether or not this will be the case can be seen by examining the effect of the specific REDOR experiment in use. Consider an I_2S REDOR experiment that starts by preparing coherence on the *I*-spins. Assuming for the moment that ω_J^{II} is zero, the system will evolve as follows for a given crystallite orientation:[48]

$$I_x^{(1)} + I_x^{(2)} \xrightarrow{\bar{\mathscr{H}}^{I_2S}(t_1)} I_x^{(1)}\cos(\Delta\phi_D^{(1)}) + I_x^{(2)}\cos(\Delta\phi_D^{(2)}) + 2I_y^{(1)} S_z \sin(\Delta\phi_D^{(1)}) + 2I_y^{(2)} S_z \sin(\Delta\phi_D^{(2)}) \quad (11)$$

The two couplings evolve independently of one another, and coherence is never transferred through the *S*-spin. Evolution is confined to these four states throughout the entire t_1 period of the REDOR experiment. The situation is different for an

S-detected REDOR experiment, where the following initial result is obtained:

$$S_x \xrightarrow{\bar{\mathscr{H}}^{I_2S}(t_1)} S_x \cos(\Delta\phi_D^{(1)}) + S_x \cos(\Delta\phi_D^{(2)}) + 2I_z^{(1)} S_y \sin(\Delta\phi_D^{(1)}) + 2I_y^{(2)} S_z \sin(\Delta\phi_D^{(2)}) \quad (12)$$

Continued evolution for suitably long t_1 periods will then yield the observable of interest:

$$S_x \cos(\Delta\phi_D^{(1)}) + S_x \cos(\Delta\phi_D^{(2)}) + 2I_z^{(1)} S_y \sin(\Delta\phi_D^{(1)}) + 2I_z^{(2)} S_y \sin(\Delta\phi_D^{(2)}) \xrightarrow{\bar{\mathscr{H}}^{I_2S}(t_1)} S_x \cos(\Delta\phi_D^{(1)}) \cos(\Delta\phi_D^{(2)}) + ... \quad (13)$$

The term on the right of eq 13, which will dominate at longer times, illustrates the effective coherence mixing between the *I*-spin states. The exact type of REDOR experiment applied to the I_2S system thus plays an important role in determining the results, as real-space interference effects will affect experiments that excite and detect the *S*-spin using the sequence of Figure 2 (top). A similar situation can arise if the homonuclear *J*-coupling evolution between the *I*-spins is appreciable on the time scale of the REDOR evolution period (i.e., ω_J^{II} is significant). An *I*-detected REDOR experiment would then experience a slower-developing interference effect. Any one of the terms in eq 11 can evolve under ω_J^{II}; here the effect is shown for the first term on the right-hand side:

$$I_x^{(1)} \cos(\Delta\phi_D^{(1)}) \xrightarrow{\bar{\mathscr{H}}_J^{I_2S}(t_1)} I_x^{(1)} \cos(\Delta\phi_D^{(1)}) \cos(\omega_J^{II} t_1) + 2I_y^{(1)} I_z^{(2)} \cos(\Delta\phi_D^{(1)}) \sin(\omega_J^{II} t_1) \quad (14)$$

$$\xrightarrow{\bar{\mathscr{H}}_D^{I_2S}(t_1)} ... + 4I_y^{(1)} I_z^{(2)} S_z \cos(\Delta\phi_D^{(1)}) \sin(\omega_J^{II} t_1) \sin(\Delta\phi_D^{(2)} t_1) + ...$$

This predicts evolution through three-spin states representing mixed dipolar and scalar order, although no additional orientational dependence is imparted by the isotropic *J*-coupling.

From the spin-space arguments of eqs 11 and 13, it is anticipated that REDOR experiments on I_2S systems will observe strong interference effects when the *S*-spin is detected and no interference effects when the *I*-spin is detected. In I_2S systems with a sufficient homonuclear *J*-coupling interaction, the *I*-detected REDOR might also be affected by a more slowly developing effect. The real-space portion of these interactions can be used to analyze the form of the interference effects.

Calculation of Interference Effects. A semianalytical derivation of the I_2S REDOR signal is useful for constructing data analysis methods. For the two-spin *IS* case, propagation of the density matrix via eqs 5−7 gives the time domain NMR signal by evaluation of the observable. After the usual averaging and weighting over a spherical distribution of powder angles, the signal observed in the REDOR experiment is obtained:

$$\frac{S}{S_0}(D_{IS}, t_1) = \frac{1}{4\pi}\int_0^{2\pi} d\alpha \int_0^{\pi} \sin\beta \, d\beta \cos[\Delta\phi_D(\alpha,\beta,t_1)] \quad (15)$$

The cosine function in eq 15 is the result of the exponential form of the propagator, and its symmetry prevents the REDOR experiment from measuring the sign of the dipolar coupling in eq 4. This expression can be integrated and simplified to yield an analytical form in terms of quarter integer-order Bessel functions:[23,51]

$$\frac{S}{S_0}(D_{IS},t_1) = \frac{\sqrt{2}\pi}{4} J_{1/4}(\sqrt{2}D_{IS}t_1) J_{-1/4}(\sqrt{2}D_{IS}t_1) \quad (16)$$

The REDOR signal is specified as the ratio of the signals from the two experiments (S/S_0), where S_0 refers to a control experiment performed without any dephasing pulses to account for the signal from uncoupled spins.[6−8] For isolated Hamiltonians of the form of eq 2, signals of the form of eq 16 are predicted. The linearity of the REDOR transform then allows for the analysis of sums or distributions of D_{IS} values.[23]

The signal can also be calculated for the case of an I_2S system in which coherence is efficiently transferred through the *S*-spin, such as that observed in the *S*-detected REDOR experiment of Figure 2 (top). This result has been previously found for any number of *I*-spins (i.e., an I_nS spin system) and is written[38]

$$\frac{S}{S_0}(t_1, D_{IS}^{(1)}...D_{IS}^{(n)}, \Omega^{(1)}...\Omega^{(n)}) = \frac{1}{(4\pi)^n}\int \prod_{i=1}^{n} \cos[\Delta\phi_D^{(i)}(\alpha^{(i)},\beta^{(i)},t_1)] \sin\beta^{(i)} \, d\Omega^{(i)} \quad (17)$$

where the integration is performed over the set of angles for each of the *n* spins (denoted by $\Omega^{(i)}$). The sum of dipolar interactions in the Hamiltonian has become a product because of the commutation of the individual dipolar interactions.[52]

A computationally usable form of eq 17 can be obtained by expressing the PAS of each dipolar interaction in a common reference frame. A vector $v_{(i)}$ is defined as the unit vector from the *S* spin to the *i*-th *I* spin. The unit vectors are then rotated relative to each other around Cartesian axes by Euler rotation matrices (**R**):[53]

$$v'_{(i)} = \mathbf{R}_z(\Phi)\mathbf{R}_y(\Theta)\mathbf{R}_z(\Psi)v_{(i)} \quad (18)$$

with angles given by Φ, Θ, and Ψ. Because the interactions will undergo a powder average over all possible orientations, a simplified arbitrary axis system is used to align the *z*-axis with the internuclear vector from spin $I^{(1)}$ to spin *S*, so that $v'_{(i)}$ is {0,0,1}. The vector $v_{(2)}$ (from spin $I^{(2)}$ to spin *S*) is a rotation about the *y*-axis by an angle γ; that is, $v_{(2)} = \mathbf{R}_y(\gamma)v_{(1)}$. Rotation of these two vectors by eq 18 results in $v'_{(1)}$ and $v'_{(2)}$:

$$v'_{(1)} = \begin{pmatrix} -\cos\Phi \sin\Theta \\ \sin\Phi \sin\Theta \\ \cos\Theta \end{pmatrix} \quad (19)$$

$$v'_{(2)} = \begin{pmatrix} -\sin\gamma\,(\cos\Phi\cos\Theta\cos\Psi - \sin\Phi\sin\Psi) - \cos\gamma\cos\Phi\sin\Theta \\ -\sin\gamma\,(-\sin\Phi\cos\Theta\cos\Psi - \cos\Phi\sin\Psi) - \cos\gamma\sin\Phi\sin\Theta \\ \cos\gamma\cos\Theta - \cos Y\sin\gamma\sin\Theta \end{pmatrix} \quad (20)$$

Projections of rotated unit vectors can be obtained from the individual interaction angles with the following substitutions: $v'_{(i)} \cdot \mathbf{x} = \cos\alpha^{(i)} \sin\beta^{(i)}$, $v'_{(i)} \cdot \mathbf{y} = \sin\alpha^{(i)} \sin\beta^{(i)}$, and $v'_{(i)} \cdot \mathbf{z} = \cos\beta^{(i)}$. Equation 10 can then be written as

$$\Delta\phi_D^{(i)}(\alpha^{(i)},\beta^{(i)},t_1) = \pm 4\sqrt{2}D_{IS}^{(i)} t_1 [v'_{(i)} \cdot \mathbf{y}][v'_{(i)} \cdot \mathbf{z}] \quad (21)$$

This expression is used to rewrite eq 17 for the I_2S spin system of interest as follows:

$$\frac{S}{S_0}(t_1,D_{IS}^{(1)},D_{IS}^{(2)},\Omega^{(1)},\Omega^{(2)}) = \frac{1}{16\pi^2}\int_0^{2\pi}\int_0^{\pi}\int_0^{2\pi}[\cos(4\sqrt{2}D_{IS}^{(1)}t_1[\nu'_{(1)}\cdot\mathbf{y}][\nu'_{(1)}\cdot\mathbf{z}]) \times \cos(4\sqrt{2}D_{IS}^{(2)}t_1[\nu'_{(2)}\cdot\mathbf{y}][\nu'_{(2)}\cdot\mathbf{z}])]\,\mathrm{d}\Phi\sin\Theta\,\mathrm{d}\Theta\,\mathrm{d}\Psi \quad (22)$$

Note that eq 22 highlights the expected difference between the REDOR signals in the I_2S and IS spin systems, in that destructive interference occurs via the product of cosines before the powder integration, depending on the orientation of the two dipolar interactions in their mutual reference frame. The change to this frame is accomplished by substitution of eqs 19−20 into eq 21 to obtain new expressions for $\Delta\phi_D^{(i)}$. It is also helpful to express the trigonometric product in eq 22 as

$$\frac{S}{S_0} = \frac{1}{8\pi^2}\int_0^{2\pi}\int_0^{\pi}\int_0^{2\pi}[\cos(\Delta\phi_D^{(1)}+\Delta\phi_D^{(2)}) + \cos(\Delta\phi_D^{(1)}-\Delta\phi_D^{(2)})]\,\mathrm{d}\Phi\sin\Theta\,\mathrm{d}\Theta\,\mathrm{d}\Psi \quad (23)$$

The values for $\Delta\phi_D^{(1)}$ and $\Delta\phi_D^{(2)}$ are then given by

$$\cos(\Delta\phi_D^{(1)}\pm\Delta\phi_D^{(2)}) = \cos[4\sqrt{2}D_{IS}^{(1)}t_1\cos\Theta\sin\Phi\sin\Theta \pm 4\sqrt{2}D_{IS}^{(2)}t_1(\cos\gamma\cos\Theta-\cos\Psi\sin\gamma\sin\Theta)(-\sin\gamma\times[-\cos\Psi\cos\Theta\sin\Phi-\cos\Phi\sin\Psi]+\cos\gamma\sin\Phi\sin\Theta)] \quad (24)$$

The form of the signal given in eqs 23 and 24 has been numerically integrated to simulate the desired I_2S REDOR signal.[22,39−40] However, computational efficiency can be improved by deriving a more compact form.[37] Trigonometric identities can be used to manipulate eq 24 so that every term in the equation contains a multiplication by a factor of either cos Φ or sin Φ:

$$\begin{aligned}\cos(\Delta\phi_D^{(1)}\pm\Delta\phi_D^{(2)}) = \cos[&2\sqrt{2}D_{IS}^{(1)}t_1\sin\Phi\sin2\Theta \\ &\pm 2\sqrt{2}D_{IS}^{(2)}t_1(\sin\Phi\sin2\gamma\cos^2\Theta\cos\Psi \\ &+\cos\Phi\sin2\gamma\sin\Psi\cos\Theta + \sin\Phi\sin2\Theta\cos^2\gamma \\ &-\sin\Phi\sin2\Theta\cos^2\Psi\sin^2\gamma - \cos\Phi\sin2\Psi\sin^2\gamma\sin\Theta \\ &-\sin\Phi\sin2\gamma\sin^2\Theta\cos\Psi)]\end{aligned} \quad (25)$$

This allows for a convenient separation of terms, so that the following relation can be used to reduce the number of powder integrals required for simulations of the signal:[54]

$$J_0(\sqrt{a^2+b^2}) = \frac{1}{2\pi}\int_0^{2\pi}\cos(a\cos\chi + b\sin\chi)\,\mathrm{d}\chi \quad (26)$$

where J_0 is the zeroth-order Bessel function of the first kind. Setting $\chi = \Phi$, the signal becomes

$$\frac{S}{S_0} = \frac{1}{4\pi}\int_0^{2\pi}\int_0^{\pi}[J_0(\sqrt{a_+^2+b^2}) + J_0(\sqrt{a_-^2+b^2})]\,\mathrm{d}\Psi\sin\Theta\,\mathrm{d}\Theta \quad (27)$$

After further trigonometric simplifications, the a and b terms are defined as

$$a_\pm = 2\sqrt{2}[D_{IS}^{(1)}t_1\sin2\Theta \mp D_{IS}^{(2)}t_1(\sin2\Theta(\cos^2\Psi\sin^2\gamma-\cos^2\gamma)\pm\cos2\Theta\cos\Psi\sin2\gamma)] \quad (28)$$

$$b = 2\sqrt{2}D_{IS}^{(2)}t_1(\cos\Theta\sin\Psi\sin2\gamma-\sin\Theta\sin2\Psi\sin^2\gamma) \quad (29)$$

The integral in eq 27 shows inversion symmetry through the center of a sphere, which restricts the integration to a hemisphere:[55]

$$\frac{S}{S_0} = \frac{1}{4\pi}\int_0^{2\pi}\int_0^{\pi/2}[J_0(\sqrt{a_+^2+b^2}) + J_0(\sqrt{a_-^2+b^2})]\,\mathrm{d}\Psi\sin\Theta\,\mathrm{d}\Theta \quad (30)$$

Equation 30 represents the final form of the I_2S signal used in the present work. A similar derivation was used to determine the effect of natural abundance spins on a long-range REDOR distance measurement.[37] The double integral exhibits superior computational performance compared to the triple integral utilized in other analyses.[39,40]

Geometry Determinations in I_2S Systems Using REDOR Experiments. The I_2S signal defined by eq 30 is a function of D_1, D_2, and γ. As noted, the intention here is to measure the dipolar couplings in a separate experiment that does not depend on the angle, to simplify the determination of γ. This is achieved by use of the S-detected θ-REDOR experiment and the complementary I-detected REDOR experiment. Other recently developed techniques would also be suitable for this task, including the improved MSREDOR experiment.[42−46] The θ-REDOR experiment has the advantage of producing a 2D-REDOR spectrum that simultaneously measures both dipolar couplings in the I_2S system in a single experiment. The experiment is based on a θ pulse, applied to the I-channel, which has the property of being unlikely to flip more than one spin. A pulse of 40° was found to be useful for the I_2S spin system studied here.[44,56] The methods of Liivak and Zax[45,46] also rely on a θ pulse (or a phase-shifted equivalent) along with additional processing and can be effectively substituted for the θ-REDOR sequence.

The theoretical results presented above, combined with the availability of θ-REDOR, suggest a procedure for structural measurements in unknown I_2S systems. The individual dipolar couplings D_1 and D_2 can be determined from an S-detected θ-REDOR or an I-detected REDOR experiment. These values are then used to obtain the angle γ via eq 30 from S-detected REDOR data. The above analysis indicates that a limitation of this approach is the ambiguity between γ and 180° − γ in the signal of eq 30, which results in identical I_2S REDOR signals for these two cases. In the experimental cases discussed here, other constraints (e.g., a chemical bond between two members of the I_2S triad) will quickly clarify the angle determination.

III. Experimental and Computational Procedures

Solid-State NMR Experiments. All experiments were performed on an 11.7 T Chemagnetics Infinity 500 spectrometer operating at spectral frequencies of 499.624, 125.635, and 50.628 MHz for ^{1}H, ^{13}C, and ^{15}N, respectively. A 5-mm triple-resonance MAS probe manufactured by Chemagnetics (model MPRB 500318) was used, and RF field strengths varied from 45 to 50 kHz for ^{13}C and ^{15}N π and θ pulses. All θ pulses were set to an estimated flip angle of 40°. Repetitive trains of π pulses were phase cycled using the XY-16 scheme.[57] Spinning rates varied from 6 to 10 kHz and were controlled to within 2 Hz of

the set value. (The REDOR pulse sequence shown in Figure 2b is known to be particularly sensitive to fluctuations in spinning rate.[58,59]) The temperature in the MAS spinning module was maintained at 25 °C. Cross-polarization from ^{1}H utilized a single linear RF power ramp of approximately 30 → 40 kHz on the *I* or *S* channel to enhance signal-to-noise and improve reproducibility.[60] Proton decoupling during the REDOR dephasing periods was performed at ~100 kHz to avoid any undesired Hartman-Hahn contact.[61] During the t_2 detection period this level was dropped to ~65 kHz. Two-pulse phase-modulated (TPPM) decoupling[62] was employed at these two power levels at all times after the cross-polarization period. This sequence has been shown to be effective in conjunction with REDOR-type experiments.[63] REDOR data points were sampled in the t_1 dimension every 2 or 4 rotor periods. Oversampling of the REDOR time domain signal (i.e., using 2 rotor period increments) was utilized in some cases as discussed below. REDOR experiments were acquired as full 2D data sets, with effective spectral widths in the dipolar (F_1) dimension ranging from 1.5 kHz to 5 kHz.

Sample Preparation. The uracil sample was prepared by mixing 10% of 2-^{13}C, $^{15}N_2$-uracil (Isotec) with natural abundance material, followed by recrystallization and drying. The sample of uniformly labeled $^{13}C_2$, ^{15}N-glycine (Isotec) was also diluted to 10% in unlabeled glycine by recrystallization. The dilution factor for these samples is sufficient to minimize contributions from intermolecular coupling to other isotopically labeled molecules. (This does not avoid the issue of coupling to natural abundance ^{13}C, which can be an issue in ^{15}N-detected REDOR experiments.) The samples were held at the center of a zirconia MAS rotor by a set of spacers to minimize the effects of RF inhomogeneity.[64]

Numerical Simulation and Processing Methods. Experimental dipolar signals were extracted from intensities along the t_1 dimension of 2D REDOR data sets after standard Fourier processing in the directly detected dimension. Theoretical signals were obtained from numerical simulations of the 1D I_2S REDOR signal in eq 30 and also from full density matrix methods. For the numerical realization of eq 30, both grid methods and the efficient REPULSION scheme were tested for the hemispherical integration.[65] It was found that signals could be rapidly simulated on PC workstations using REPULSION angle sets with 2500 elements; therefore, all signals simulated with eq 30 made use of this angle set. Full density matrix simulations of I_2S REDOR signals (i.e., using eq 7) were carried out using a programmable simulator written in the Fortran-90 language. The simulator allows for rotations between the PAS of dipolar interactions and other relevant axis systems. A synchronously detected 1D version of the REDOR sequence[7] was simulated using time-dependent MAS propagators calculated from small finite time-independent increments of 1−2 μs. The powder integration was limited to 500 REPULSION elements for full density matrix simulations because of their complexity and the requirement for an additional rotor position angle.

Both the REDOR transform[23] and Tikhonov regularization[24] procedures were used to process time domain REDOR signals, after multiplication with a three-point Blackman−Harris window function[66] and zero-filling (unless otherwise noted). The model-free REDOR transform was used for simulated data. The dipolar spectrum $F(D)$ is computed from the time domain data $f(t)$ via a discrete form of the following integral transform:

$$F(D) = \int_{t_1}^{t_2} K^{-1}(D,t) f(t)\, \mathrm{d}t \tag{31}$$

where the kernel function K^{-1} is the analytical inverse of eq 16.[23,24] The Tikhonov regularization procedure is somewhat more complex and is primarily intended for experimental data. Tikhonov regularization extracts $F(D)$ from the modified problem

$$f(t) = \int_{D_1}^{D_2} K(D,t) F(D)\, \mathrm{d}D + \epsilon(t) \tag{32}$$

where experimental noise has been explicitly introduced as $\epsilon(t)$. The kernel K is the function given in eq 16, and the inverse is found numerically by minimization of a linear least-squares function Γ:[67]

$$\Gamma\left(\lambda\right) = \sum_{j=1}^{n} \frac{1}{\sigma_j}\left((f_j + \epsilon_j) - \int_{D_1}^{D_2} K(D,t) F(D)\, \mathrm{d}D\right)^2 + \lambda ||\mathbf{D}F\left(D\right)||_2 \tag{33}$$

where **D** is the second-derivative operator, $(f_j + \epsilon_j)$ represents the sum of the time domain signal and the noise, and σ_j is determined by the noise model. The regularization procedure is especially useful for experimental data because it stabilizes the solution in the presence of noise via the second-derivative smoothing functional, which is scaled by the parameter λ. Further details of the calculation have been previously described.[24,67] Optional positivity constraints are supported by the regularization procedure but were only enabled if the signal was expected to arise solely from *IS* spin pairs (as in a θ-REDOR experiment).

I_2S REDOR signals were fit to eq 30 using standard nonlinear Levenburg−Marquardt methods.[68] The fits were carried out in both the time and frequency domains to determine the angle γ. An analysis of the angular precision for γ was made using minimum variance or Cramér−Rao lower bounds (CRLB).[25] The noise level was calculated from the experimental data by comparison with signals simulated using the best fit of γ and the known dipolar coupling constants. The residuals from this comparison were fit to a Gaussian noise function. From the signal in eq 30, using derivatives calculated by the finite difference method, the Fisher information matrix was found and scaled by the noise level to determine the CRLB and the precision of the nonlinear fitting results.

IV. Results and Discussion

Geometry Determination for Uracil. The 2-^{13}C, $^{15}N_2$-uracil molecule, shown in Figure 3a, contains the basic I_2S spin system of interest and was used as an initial test of the proposed method. (The negligible two-bond homonuclear ^{15}N-^{15}N *J*-coupling in uracil can be conveniently ignored here; this coupling was observed to be 2.6 Hz in d_6-DMSO solution, which is similar to other reported values.[69]) The results of three separate REDOR experiments on the uracil sample, after transformation into dipolar spectra, are shown in Figures 3b−e. Figure 3b shows the results of an *S*-detected (S = ^{13}C) REDOR experiment performed at a 10 kHz MAS rate with sampling every two rotor periods. This substantial oversampling of the dipolar signal was necessitated by its rapid decay. A total of 64 REDOR points were acquired, and the data were processed by Tikhonov regularization after apodization and zero-filling. Positivity constraints were not employed since negative excursions are possible for dipolar transformed I_2S REDOR signals. The broad pattern observed in Figure 3b contains information about the orientation of the dipolar interactions, which can be extracted by comparison with the theoretically predicted signals, as demonstrated below.

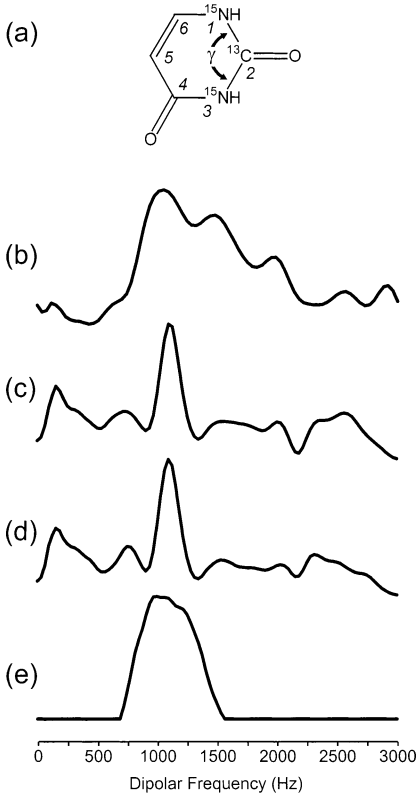

Figure 3. Results of the REDOR experiments on 2-^{13}C, $^{15}N_2$-uracil. (a) Structure of the uracil molecule showing the isotopic labeling scheme and the angle of interest. (b) Dipolar spectrum obtained from Tikhonov regularization (after apodization and zero-filling) of a ^{13}C-detected ($S = {}^{13}$C) REDOR experiment on the uracil sample (see text). (c) Results of a ^{15}N-detected ($I = {}^{15}$N) REDOR experiment (upfield ^{15}N signal), processed as in (b). (d) As in (c), but the signal from the downfield ^{15}N resonance. (e) The dipolar spectrum from a ^{13}C-detected θ-REDOR experiment, processed as before except with positivity constraints enabled for the Tikhonov procedure (since spin-pair behavior is expected in this experiment). Note that the data set shown in (b) was acquired at a 10 kHz MAS rate, while all other data sets were acquired at 8 kHz. In all cases, REDOR sampling was performed every two rotor periods, and 64 points were acquired. The three separate 2D-REDOR experiments used to produce these data each required approximately 1 day of experimental time.

A second 2D-REDOR experiment was performed on the uracil sample using *I*-detection ($I = {}^{15}$N). This resulted in similar dipolar dephasing behavior for both ^{15}N resonances. The processed dipolar spectra for these signals are shown in Figures 3c and d for the upfield and downfield resonances, respectively. The longer time domain decay that was observed allowed for a slower MAS rate (8 kHz) and sampling every second rotor period (4 kHz spectral width). From the dipolar spectra the two *IS* internuclear distances in uracil are seen to be indistinguishable. The additional spectral intensity at low dipolar frequencies may be due to multiple-spin effects from distributed natural-abundance ^{13}C spins at longer distances. (This problem is most noticeable for ^{15}N-detection because of the greater molar content of ^{13}C in organic compounds.) In addition, a ^{13}C-detected θ-REDOR experiment was also performed on this material under the same conditions as the *I*-detected REDOR experiment. The processed dipolar spectrum is shown in Figure 3e. The Tikhonov regularization procedure was again employed, now using positivity constraints, since this spectrum is theoretically expected to represent spin pairs. The additional broadening of the peak (in comparison to the ^{15}N-detected data) is probably caused by the particular θ-REDOR sequence used here, in which the imperfect refocusing of a large number of spin−echoes can lead to an additional loss of signal intensity and a broadening of the dipolar peak.[58] Despite this broadening, the ^{13}C-detected θ-REDOR spectrum does have an advantage over ^{15}N-detection, since it is affected to a lesser extent by natural-abundance background problems. In this case the experiments yielded the same dipolar coupling, but in more complicated studies there may be a preferred detection scheme.

The values of γ, r_1, and r_2 and hence the geometry of the I_2S cluster can be determined from the data in Figure 3. Both the θ-REDOR and ^{15}N-detected experiments indicate dipolar couplings of 1090 Hz and a distance of 1.41 Å (eq 4). This compares favorably to the results of an X-ray crystallography study, which found two similar carbon−nitrogen distances of 1.371 and 1.376 Å.[70] The distances determined by these two methods usually differ by about 3%, due to the effects of dynamic phenomena.[71,72] The angle γ can be obtained by nonlinear fitting of the experimental signal to the theoretical signal of eq 30 in both the time domain and the dipolar domain. The nonlinear fit with CRLB error estimation in the dipolar domain, using the data in Figure 3b, indicated a γ value of 113.4° ± 0.5°. The time domain fit resulted in a γ value of 112.1° ± 0.9°. The determination of γ can also be visualized, in an approximate way, by contour plots showing the signal as a function of γ for $D_1 = D_2 = 1090$ Hz (Figure 4). Inspection of these surfaces indicates that the signal is distinctly dependent on γ. Stronger features are observed on the dipolar-transformed surface as compared to the time domain signals. This may have enhanced the precision of the fit in this case (as discussed below). Note that visual comparison of the experimental data with these simulated sets indicates two possibilities for γ of ∼66° and ∼114° as expected from eq 30. Knowledge of the six-membered ring structure of uracil and the isotopic labeling scheme immediately rules out the former angle. The contour plots in Figure 4 provide good starting points for nonlinear fitting while helping to identify potentially confusing I_2S interference effects.

The angles obtained from the nonlinear fitting, especially the result in the dipolar domain ($\gamma = 113.4° \pm 0.5°$), are in good agreement with the value reported in the most recent X-ray crystallographic study of crystalline uracil ($\gamma = 114.0° \pm 0.1°$).[70] (Note that this study superseded earlier work,[73] which had indicated a different value of 115.6°.) Electron diffraction data on gas-phase uracil also obtained a similar result of 114.6° ± 2.0°.[74] The REDOR results given here compare favorably with these values and are relatively precise. A close agreement between X-ray crystallography and solid-state NMR can be expected, as vibrational effects do not affect angle determinations as strongly as distance determinations.[72] In addition, the somewhat predictable and equal enhancement of dipolar coupling constants simply scales the interference pattern and is thus unlikely to affect the angular analysis.

The experimental results for uracil also support the theoretical expectations, in that the predictable effect of interference between the dipolar tensors can be used to precisely determine γ. Figure 5 presents a comparison of the experimental spectrum with simulated spectra produced for $\gamma = 113.4°$ using eq 30 and a full density matrix calculation. The density matrix simulation took into account the effects of the two heteronuclear dipolar interactions present in the I_2S subsystem. The experimental RF power levels of 45 kHz and a spinning rate of 10 kHz were also used in the simulation, although all other interactions and natural-abundance nuclei (including protons) were ignored, as were the effects of RF inhomogeneity. The

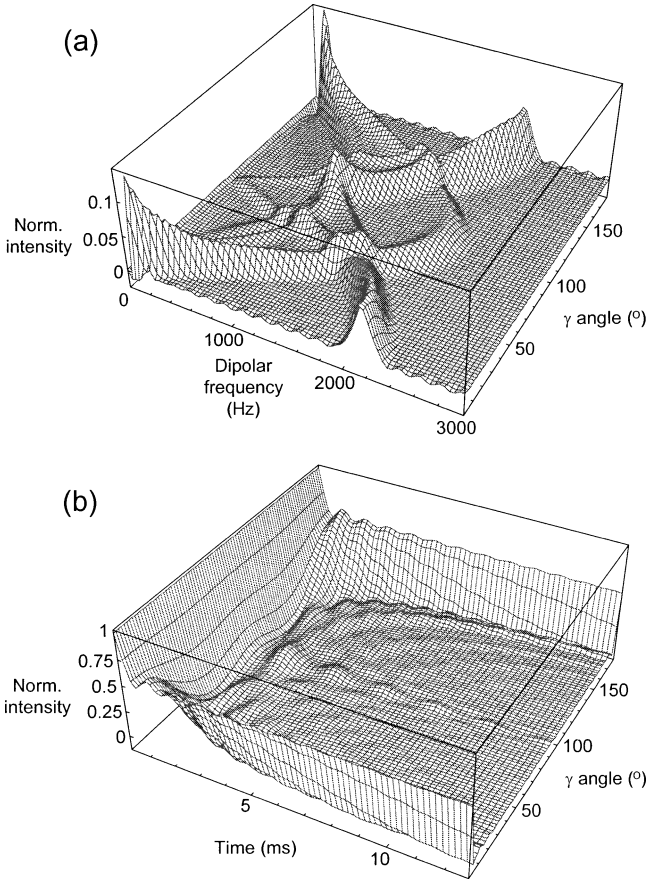

Figure 4. Visualizations of the effects of γ on the *S*-detected I_2S REDOR signal for 2-^{13}C, $^{15}N_2$-uracil. The simulated signals were generated by integration of eq 30 with $D_1 = D_2 = 1090$ Hz. In (a), the dipolar spectrum (after apodization and REDOR transformation) as a function of γ is shown. The area under each spectrum was normalized to unity. The strong dependence of the spectral features on γ is evident and illustrates how the REDOR transform can be used to help identify the presence of an I_2S system. In (b), the results of the simulation are presented in the time domain without additional processing (with the first data points normalized to unity). The features are also strongly affected by the value of γ, but the effects appear to be less pronounced. By a visual comparison, the experimental data obtained from uracil are seen to be most consistent with slices of these maps taken at ~66° and ~114°. The angle was fit to 113.4° ± 0.5° in the dipolar domain and 112.1° ± 0.9° in the time domain.

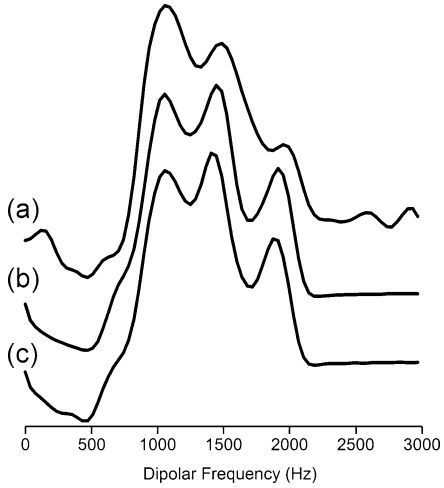

Figure 5. Comparison of the experimental and theoretically simulated dipolar spectra for uracil. The experimental data are shown in (a) and are compared with data simulated using eq 30 in (b) and with the results of a full density matrix simulation in (c). The simulations used $D_1 = D_2 = 1090$ Hz and $\gamma = 113.4°$ (see text).

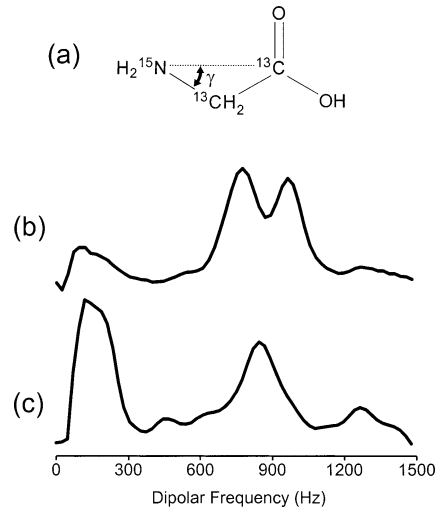

Figure 6. Results of the REDOR experiments on 1,2-^{13}C, ^{15}N-glycine. (a) Structure of the glycine molecule showing the isotopic labeling scheme and the angle of interest. (b) The dipolar spectrum obtained from Tikhonov regularization (after apodization and zero-filling) of a ^{15}N-detected ($S = {}^{15}$N) REDOR experiment on the glycine sample (see text). (c) Results of an ^{15}N-detected θ-REDOR experiment, processed as in (b). Each REDOR experiment required 1 day of experimental time.

results indicate a good level of agreement between theory and experiment for the case of uracil.

Geometry Determination for Glycine. The I_2S system in the uracil molecule is characterized by nearly equal dipolar couplings and a relatively large γ value. A considerably different case is that of 1,2-^{13}C, ^{15}N-glycine, which possesses two unequal dipolar couplings and a small γ angle. The results of REDOR and θ-REDOR experiments on the glycine sample are shown in Figure 6. (Note that the *S* spin of the I_2S system is now a ^{15}N nucleus.) The 1,2-^{13}C, ^{15}N-glycine sample exhibits a nonnegligible 53 Hz ^{13}C-^{13}C *J*-coupling (directly observable in CP-MAS spectra), which as previously noted complicates the results of *I*-detected REDOR experiments. Because of this, *I*-detected REDOR is not employed for glycine; the determination of γ can still proceed as before using the *S*-detected experimental results shown in Figures 6b and c. Each 2D-REDOR experiment acquired 32 data points in the dipolar dimension, which were processed by the Tikhonov regularization method after zero-filling and apodization. The θ-REDOR results indicate two couplings of 188 and 867 Hz. The resulting distances, which are 2.56 and 1.52 Å, respectively, are in agreement with X-ray crystallographic values of 2.48 and 1.48 Å.[75] The differences between the techniques can again be attributed to motional effects.[71,72] From these couplings the angle can be estimated by comparison of the experimental data in Figure 6b with simulated spectra as a function of angle, as shown in Figure 7. The spectra at γ values of ~34° and ~146° bear the most resemblance to the experimental interference pattern. The second of these angles is unlikely given the chemical structure of glycine and the known isotopic labeling scheme, since it would require a highly improbable carbon−carbon bond length. The achievable precision of this method is quantified by a nonlinear fit and CRLB analysis to yield $\gamma = 34.7° \pm 0.7°$ (in the dipolar domain) and $\gamma = 33.6° \pm 1.9°$ (in the time domain). These values compare favorably with the crystallographic result of $\gamma = 33.5°$.[75] A direct comparison of the experimental and simulated spectra with a full density matrix

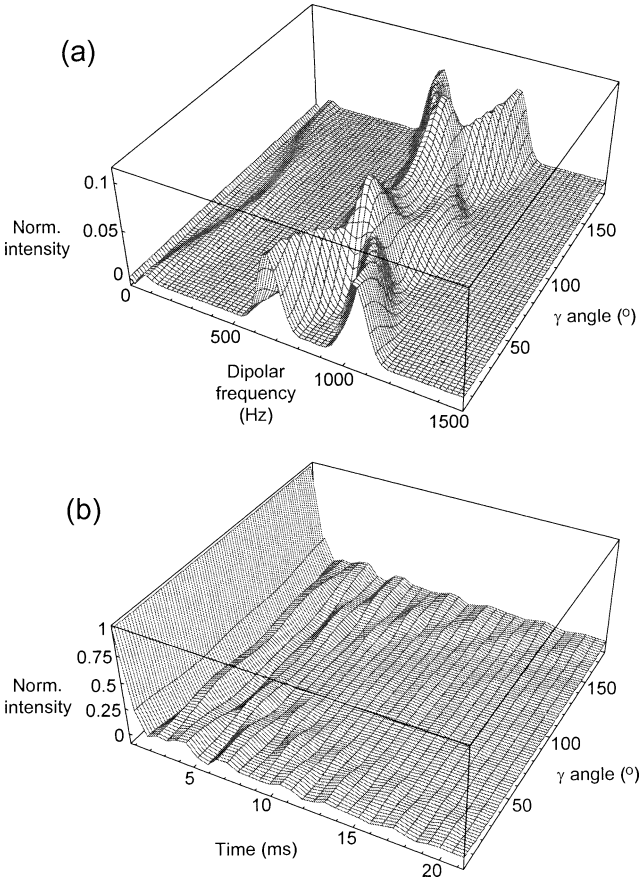

Figure 7. Visualizations of the effects of γ on the *S*-detected I_2S REDOR signal for 1,2-^{13}C, ^{15}N-glycine. The simulated signals were generated by integration of eq 30 with $D_1 = 188$ Hz and $D_2 = 867$ Hz. In (a), the dipolar spectrum (after apodization and REDOR transformation) as a function of γ is shown (with the area under each spectrum normalized to unity). The dependence of the spectral features on γ is significant, as seen in Figure 4. In (b), the results of the simulation are presented in the time domain without additional processing (with the first data points normalized to unity). By a visual comparison, the experimental data obtained from glycine are seen to be most consistent with slices of the map taken at ~34° and ~146°. The latter value is ruled out by bonding arguments (see text). The angle was fit to $\gamma = 34.7° \pm 0.7°$ in the dipolar domain and $\gamma = 33.6° \pm 1.9°$ in the time domain.

simulation is shown in Figure 8. The experimental results correlate closely with the theoretical predictions.

Precision of the Angular Determination. Previous REDOR-based angular measurements on I_2S systems indicated an achievable precision in the range of $\pm$ 4° to $\pm$ 10°.[39,40] From the experimental results presented here, it appears that more reliable results in the vicinity of $\pm$ 1° are obtainable. The independent determination of distances and the resulting use of a single variable in the nonlinear fit are clearly the most important factors in improving the precision. The dipolar transform and regularization analyses may also contribute to the performance in some cases, because of the potential sensitivity of the dipolar transform to slight differences in γ. This sensitivity has been previously reported, as have analogous effects in the Fourier transform analysis of dipolar signals.[25,40,44] The CRLB error estimates from the uracil and glycine data empirically indicate a slightly better precision when the nonlinear fit is conducted using dipolar-transformed data. Although the results were improved in these two cases, the use of the REDOR transform and Tikhonov regularization may not always be the best approach. A much more thorough analysis

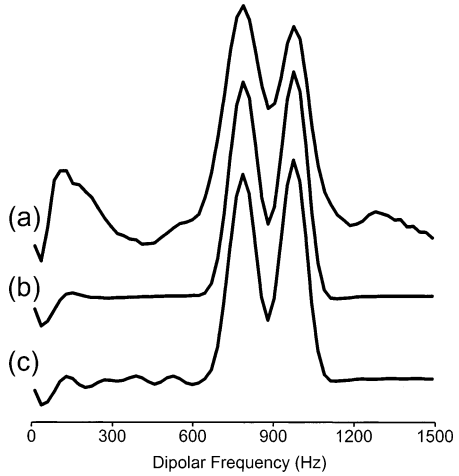

Figure 8. Comparison of the experimental and theoretically simulated dipolar spectra for glycine. The experimental data are shown in (a) and are compared with data simulated using eq 30 in (b) and with the results of a full density matrix simulation in (c). The simulations used $D_1 = 188$ Hz, $D_2 = 867$ Hz and $\gamma = 34.7°$.

is needed to better characterize the situation, since it depends in a complex and nonlinear manner on the dipolar coupling values, γ, and other experimental parameters. An error analysis of this type is currently being developed for multiple-spin REDOR signals.[76,77] Nevertheless, although the use of dipolar transforms may not always enhance the angular determination, they provide insight into the multiple-spin effects that could be present in experimental data. An example of this is given in the next section.

The acquisition of the REDOR signal can also affect the precision to which γ is determined in both the time and dipolar frequency domains. In Figure 9, a series of transformed simulated signals are shown to illustrate this point. The interference pattern becomes more detailed and refined as the number of points in the simulation increases. Unfortunately, the fast decay of the typical I_2S REDOR signal puts a very finite limit on the number of points that can be acquired before the noise level exceeds that of the signal. However, an optimal choice of sampling interval and spinning rate can help. Oversampling can be used to acquire the maximum number of REDOR data points before the noise overwhelms the signal (as in the experimental uracil data), so that the signal in both the time and dipolar domains can be more reliably analyzed.

Additional Characteristics of I_2S REDOR Signal Analysis. Several detailed points about the I_2S REDOR signal and its interaction with the dipolar transform methods are now briefly considered. As noted above, the dipolar spectra shown here, both experimental and simulated, generally display features that indicate a multiple-spin problem is present. However, in the study of unknown spin systems, a small number of REDOR points or a nearly linear γ angle could render these features unobservable. Comparison of the dipolar spectrum with that obtained from a θ-REDOR experiment may still clarify the issue. In any case, when enough data points are available, the multiple-spin effects observed in the dipolar spectra are a fundamental property of the I_2S signal, and do not result from apodization (as proposed in previous work).[40] Although the interference effects are studied here by a data processing method designed for *IS* spin systems, both theory and experiment indicate that the interpretation of dipolar spectra from I_2S REDOR experiments as "distance" spectra is not appropriate.[40]

The rationale behind the use of dipolar transforms as a general analysis tool for I_2S REDOR signals is best demonstrated by

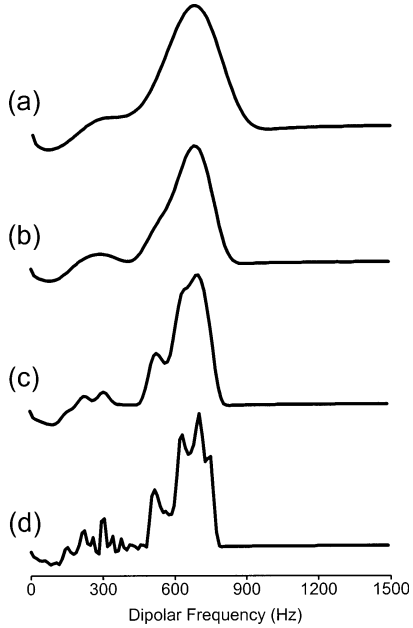

Figure 9. Demonstration of resolution effects on dipolar spectra. As more REDOR points are taken, the features of the dipolar spectrum sharpen and become highly defined. Test signals were generated using $D_1 = 300$ Hz, $D_2 = 600$ Hz, $\gamma = 50°$, and a spectral width of 1500 Hz. All spectra consist of a total of 128 points, with the first n points simulated via eq 30 and the remaining $(128 - n)$ points set to zero. The REDOR transform of the signals is shown for (a) $n = 16$, (b) $n = 32$, (c) $n = 64$, and (d) $n = 128$. Although the maximum number of points obtainable in a REDOR experiment is limited, these results suggest that obtaining as many points as possible will increase the precision in the determination of γ.

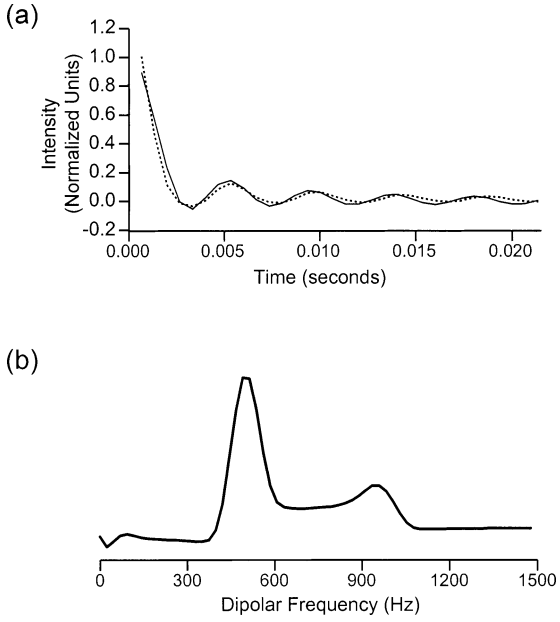

Figure 10. I_2S REDOR signal for $D_1 = D_2$ and $\gamma = 90°$. (a) The dashed line represents 32 points of time domain I_2S REDOR data simulated via eq 30 with $D_1 = D_2 = 500$ Hz. A spectral width of 1500 Hz was used. The solid line is a time domain fit of this simulated I_2S signal to the two-spin signal in eq 16 (see text). (b) REDOR transform of the simulated $\gamma = 90°$ data, which clearly shows dipolar interference.

an example. A recent study reported that a special case occurs when $D_1 = D_2$ and $\gamma = 90°$, such that the signal measured is equivalent to that from a single *IS* coupling equal to $\sqrt{2}D_1$.[40] Simulations using eq 30 and full density matrix calculations do not show this to be the case. For example, in Figure 10(a), the dashed line represents a simulated signal generated using eq 30 with $D_1 = D_2 = 500$ Hz and $\gamma = 90°$. This time domain form does resemble a single *IS*-type signal of the form of eq 16. A simple time domain fit to this signal shows what may be the reason for the confusion, as the signal fits fairly well to eq 16 with $D = 522$ Hz [the thin solid line in Figure 10a]. (This value still differs substantially from the 707 Hz predicted by $\sqrt{2}D_1$.) In any case, a number of significant deviations are observed between these two simulated signals at both short and long times. In Figure 10b, a REDOR transform analysis clearly shows the true nature of the $\gamma = 90°$ signal to be the expected dipolar interference pattern. The strongest peak in this spectrum corresponds to the D of 522 Hz obtained from the fit. This example highlights the features that can be missed when a time domain analysis is used without the benefit of dipolar transforms.

Another special case of the I_2S signal is seen when $D_1 = D_2$ and $\gamma = 0°$ or 180°.[40] In this case the dipolar interactions share the same PAS, and the theoretical I_2S signal oscillates at $D_1 + D_2$ and decays to a constant offset that is half that of the REDOR signal at $t = 0$. This special case is also of interest here because the offset engenders the most pathological behavior of the dipolar analysis methods, by convoluting the signal with a box function and enhancing the ill-posed nature of the REDOR transform kernel.[24] The result of this effect is demonstrated in Figure 11, where a time domain signal simulated using $D_1 = D_2 = 500$ Hz and $\gamma = 0°$ is shown in (a). The REDOR transform of this simulated signal (after apodization and zero-filling) in Figure 11b shows a number of undesired oscillations in the baseline, and the lower frequency peak is at 47 Hz instead of the expected 0 Hz. The first of these problems can be avoided by using Tikhonov regularization, at the cost of added complexity of processing, as shown in Figure 11c, where the oscillations are suppressed by the smoothing functional. The unexpected position of the lower frequency peak is caused by the use of apodization functions and is again fundamentally the result of the ill-posed nature of the problem.[24] (The deleterious effects of apodization are limited to couplings that are very small with respect to the spectral width, and thus are not a issue in most applications of the dipolar transforms, since careful time-domain analysis is usually employed for extreme-range dipolar distance measurements).[37] The problem can be avoided by use of the Tikhonov procedure *without* prior apodization and zero-filling, as in Figure 11d. The peak is now observed at a true zero frequency, although the oscillations are still observed, even with an extremely high value of the regularization parameter ($\lambda > 0.1$). A stronger smoothing functional is necessary for total suppression of the oscillations. The special case of $D_1 = D_2$ and $\gamma = 0°$ or 180° is unlikely to be of concern in practical angle measurements but can affect simulated data sets. For example, the shifted zero peak and baseline oscillations are observable in the uracil simulations of Figure 4a.

V. Conclusions

The present work has demonstrated the potential of REDOR for precise angular determinations on labeled I_2S spin systems. An *S*-detected θ-REDOR or an *I*-detected REDOR experiment is used for independent measurement of the two internuclear distances. An *S*-detected REDOR experiment, which is shown to be sensitive to γ in a predictable way, was then employed to find the angle between the internuclear vectors. Experimental measurements were made on two small polycrystalline organic molecules with a precision approaching that possible in crystallographic studies. Angular measurements of this sort may be

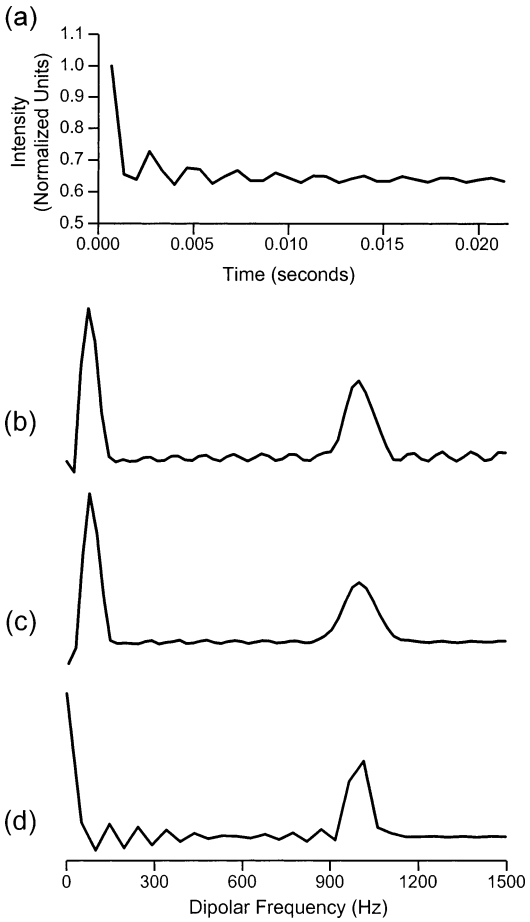

Figure 11. I_2S REDOR signal for $D_1 = D_2$ and $\gamma = 0°$ or 180°. (a) Time domain signal simulated using eq 30. Note the constant offset of the signal and its decay to approximately 60−65% of its initial intensity. This is because the point at $t = 0$ is not included in the simulation; when it is included, the normalized signal decays to 50% of its initial intensity. (b) REDOR transform of the data in (a) after apodization and zero-filling. (c) Tikhonov regularization of the data in (a), again after apodization and zero-filling. The fluctuations in the baseline are suppressed by the smoothing operator. (d) Data processed using the Tikhonov method but without apodization or zero-filling. The signal is now observed at the correct frequencies, but with some remaining baseline fluctuations caused by the mathematical nature of the problem (see text).

applicable to a variety of materials, including amorphous solids, as long as an I_2S spin system is present. The two ambiguous values that can be obtained for γ may cause a problem in some cases, especially when γ and $180° - \gamma$ are close in value. In more challenging situations, additional homonuclear dipolar methods[9] (possibly in conjunction with shift tensor analysis[27−33]) or alternative labeling schemes may be necessary. Although the determination of γ was observed to yield precise results in the experimental I_2S systems examined here, further characterization of the precision as a function of γ, D_1, and D_2 is necessary to fully understand the situation. In particular, the analysis of I_2S signals at lower dipolar coupling values (<200 Hz) will help define the limits of the technique. Further examination of the data processing methods (dipolar transforms vs time domain analysis) is needed to characterize their precision. The present work has shown that both methods are reliable and that dipolar transforms are especially useful for identifying the presence of multispin effects. Extensions of this work to higher-order I_nS or I_nS_m spin systems may be possible in certain cases, which could be identified by theoretical analysis.[39] Applications of the basic I_2S REDOR methods to more complex and interesting systems, including glasses and isotopically labeled biomolecules, are currently being explored.

Acknowledgment. This report is based upon research supported by the American Cancer Society (Research Project Grant 98-174-01-CDD). The 500 MHz NMR spectrometer was obtained with the assistance of the National Science Foundation (Grant CHE-9601572). The authors also thank Dr. A. J. Benesi of the Penn State NMR Facility for helpful discussions.

References and Notes

(1) Andrew, E. R.; Bradbury, A.; Eades, R. G. *Nature* **1959**, *183*, 1802.
(2) Lowe, I. J. *Phys. Rev. Lett.* **1959**, *2*, 285.
(3) Stejskal, E. O.; Memory, J. D. *High-Resolution NMR in the Solid State*; Oxford University Press: New York, 1994.
(4) Pines, A.; Gibby, M. G.; Waugh, J. S. *J. Chem. Phys.* **1973**, *59*, 569.
(5) Stejskal, E. O.; Schaefer, J.; Waugh, J. S. *J. Magn. Reson.* **1977**, *28*, 105.
(6) Gullion, T.; Schaefer, J. *J. Magn. Reson.* **1989**, *81*, 196.
(7) Gullion, T.; Schaefer, J. *Adv. Magn. Reson.* **1989**, *13*, 57.
(8) Gullion, T. *Magn. Reson. Rev.* **1997**, *17*, 83.
(9) Bennett, A. E.; Griffin, R. G.; Vega, S. *NMR* **1994**, *33*, 1.
(10) Pan, Y.; Gullion, T.; Schaefer, J. *J. Magn. Reson.* **1990**, *90*, 330.
(11) Marshall, G. R.; Beusen, D. D.; Kociolek, K.; Redlinski, A. S.; Leplawy, M. T.; Pan Y.; Schaefer, J. *J. Am. Chem. Soc.* **1990**, *112*, 963.
(12) Garbow, J. R.; McWherter, C. A. *J. Am. Chem. Soc.* **1993**, *115*, 238.
(13) Garbow, J. R.; Breslav, M.; Antohi, O.; Naider, F. *Biochemistry* **1994**, *33*, 10094.
(14) Anderson, R. C.; Gullion, T.; Joers, J. M.; Shapiro, M.; Villhauer, E. B.; Weber, H. P. *J. Am. Chem. Soc.* **1995**, *117*, 10546.
(15) Naito, A.; Nishimura, K.; Kimura, S.; Tuzi, S.; Aida, M.; Yasuoka, N.; Saitô, H. *J. Phys. Chem.* **1996**, *100*, 14995.
(16) Nishimura, K.; Naito, A.; Tuzi, S.; Saitô, H.; Hashimoto, C.; Aida, M. *J. Phys. Chem. B* **1998**, *102*, 7476.
(17) Holl, S. M.; Marshall, G. R.; Beusen, D. D.; Kociolek, K.; Redlinski, A. S.; Leplawy, M. T.; McKay, R. A.; Vega, S.; Schaefer, J. *J. Am. Chem. Soc.* **1992**, *114*, 4830.
(18) Wooley, K. L.; Klug, C. A.; Tasaki, K.; Schaefer, J. *J. Am. Chem. Soc.* **1997**, *119*, 53.
(19) Mueller, D. D.; Schmidt, A.; Pappan, K. L.; McKay, R. A.; Schaefer, J. *Biochemistry* **1995**, *34*, 5597.
(20) Quist, P. O.; Förster, H.; Johnels, D. *J. Am. Chem. Soc.* **1997**, *119*, 5390.
(21) Lee, P. L.; Schaefer, J. *Macromolecules* **1995**, *28*, 1921.
(22) Fyfe, C. A.; Lewis, A. R.; Chezeau, J. M.; Grodney, H., *J. Am. Chem. Soc.* **1997**, *119*, 12210.
(23) Mueller, K. T.; Jarvie, T. P.; Aurentz, D. J.; Roberts, B. W. *Chem. Phys. Lett.* **1995**, *242*, 535.
(24) Vogt, F. G.; Aurentz, D. J.; Mueller, K. T. *Mol. Phys.* **1998**, *95*, 907.
(25) Hodgkinson, P.; Emsley, L. *J. Magn. Reson.* **1999**, *139*, 46.
(26) Jarvie, T. P.; Went, G. T.; Mueller, K. T. *J. Am. Chem. Soc.* **1996**, *118*, 5330.
(27) Hong, M.; Gross, J. D.; Griffin, R. G. *J. Phys. Chem. B* **1997**, *101*, 5869.
(28) Hong, M.; Gross, J. D.; Hu, W.; Griffin, R. G. *J. Magn. Reson.* **1998**, *135*, 169.
(29) Feng, X.; Verdegem, P. J. E.; Lee, Y. K.; Sandström, D.; Edén, M.; Bovee-Geurts, P.; de Grip, W. J.; Lugtenburg, J.; de Groot, H. J. M.; Levitt, M. H. *J. Am. Chem. Soc.* **1997**, *119*, 6853.
(30) Feng, X.; Edén, M.; Brinkmann, A.; Luthman, H.; Eriksson, L.; Gräslund, A.; Antzutkin, O. N.; Levitt, M. H. *J. Am. Chem. Soc.* **1997**, *119*, 12006.
(31) Gregory, D. M.; Mehta, M. A.; Shiels, J. C.; Drobny, G. P. *J. Chem. Phys.* **1997**, *107*, 28.
(32) Bower, P. V.; Oyler, N.; Mehta, M. A.; Long, J. R.; Stayton, P. S.; Drobny, G. P. *J. Am. Chem. Soc.* **1999**, *121*, 8373.
(33) Blanco, F. J.; Tycko, R. *J. Magn. Reson.* **2001**, *149*, 131.
(34) Goetz, J. M.; Schaefer, J. *J. Magn. Reson.* **1997**, *129*, 222.
(35) Andrew, E. R.; Bersohn, R. *J. Chem. Phys.* **1950**, *18*, 159.
(36) Naito, A.; Nishimura, K.; Tuzi, S.; Saitô, H. *Chem. Phys. Lett.* **1994**, *229*, 506.
(37) Arshava, B.; Breslav, M.; Antohi, O.; Stark, R. E.; Garbow, J. R.; Becker, J. M.; Naider, F. *Solid State NMR* **1999**, *14*, 117.
(38) Goetz, J. M.; Schaefer, J. *J. Magn. Reson.* **1997**, *127*, 147.
(39) Nishimura, K.; Naito, A.; Tuzi, S.; Saitô, H. *J. Phys. Chem. B* **1999**, *103*, 8398.
(40) Fyfe, C. A.; Lewis, A. R. *J. Phys. Chem. B* **2000**, *104*, 48.

(41) Bertmer, M.; Eckert, H. *Solid State NMR* **1999**, *15*, 139.
(42) Pan, Y.; Schaefer, J. *J. Magn. Reson.* **1990**, *90*, 341.
(43) Bennett, A. E.; Rienstra, C. M.; Lansbury, P. T.; Griffin, R. G. *J. Chem. Phys.* **1996**, *105*, 10289.
(44) Gullion, T.; Pennington, C. H. *Chem. Phys. Lett.* **1998**, *290*, 88.
(45) Liivak, O.; Zax, D. B. *J. Chem. Phys.* **2000**, *113*, 1088.
(46) Liivak, O.; Zax, D. B. *J. Chem. Phys.* **2001**, *115*, 402.
(47) Maricq, M. M.; Waugh, J. S. *J. Chem. Phys.* **1979**, *70*, 3300.
(48) Hing, A. W.; Vega, S.; Schaefer, J. *J. Magn. Reson. A* **1993**, *103*, 151.
(49) Jaroniec, C. P.; Tounge, B. A.; Rienstra, C. M.; Herzfeld, J.; Griffin, R. G. *J. Am. Chem. Soc.* **1999**, *121*, 10237.
(50) Gullion, T.; Vega, S. *Chem. Phys. Lett.* **1992**, *194*, 423.
(51) Mueller, K. T. *J. Magn. Reson. A* **1995**, *113*, 81.
(52) Slichter, C. P. *Principles of Magnetic Resonance*, 3rd ed.; Springer-Verlag: Berlin, 1990.
(53) Arfken, G. B.; Weber, H. J. *Mathematical Methods for Physicists*, 4th ed.; Academic Press: San Diego, 1995.
(54) Prudnikov, A. P.; Brychkov, Y. A.; Marichev, O. I. *Integrals and Series*, *Vol. 2. Special functions;* Gordon and Breach: New York, 1986.
(55) Edén, M.; Levitt, M. H. *J. Magn. Reson.* **1998**, *132*, 220.
(56) Cull, T. S.; Joers, J. M.; Gullion, T.; Norberg, R. E.; Conradi, M. S. *J. Magn. Reson.* **1998**, *133*, 352.
(57) Gullion, T.; Baker, D. B.; Conradi, M. S. *J. Magn. Reson.* **1990**, *89*, 479.
(58) Garbow, J. R.; Gullion, T. *Chem. Phys. Lett.* **1992**, *192*, 71.
(59) Chopin, L.; Rosanske, R.; Gullion, T. *J. Magn. Reson. A* **1996**, *122*, 237.
(60) Metz, G.; Wu, X.; Smith, S. O. *J. Magn. Reson. A* **1994**, *110*, 219.
(61) Ishii, Y.; Ashida, J.; Terao, T. *Chem. Phys. Lett.* **1995**, *246*, 439.
(62) Bennett, A. E.; Rienstra, C. M.; Auger, M.; Lakshmi, K. V.; Griffin, R. G. *J. Chem. Phys.* **1995**, *103*, 6951.
(63) Mitchell, D. J.; Evans, J. N. S. *Chem. Phys. Lett.* **1998**, *292*, 656.
(64) Campbell, G. C.; Galya, L. G.; Beeler, A. J.; English, A. D. *J. Magn. Reson. A* **1995**, *112*, 225.
(65) Bak, M.; Nielsen, N. C. *J. Magn. Reson.* **1997**, *125*, 132.
(66) Harris, F. J. *Proc. IEEE* **1978**, *66*, 51.
(67) Weese, J. *Comput. Phys. Commun.* **1992**, *69*, 99.
(68) Press, W. H.; Flannery, B. P.; Teukolsky, S. A.; Vetterling, W. T. *Numerical Recipes in C*, 2nd ed.; Cambridge University Press: Cambridge, 1991.
(69) Berger; S.; Braun, S.; Kalinowski, H. O. *NMR Spectroscopy of the Non-Metallic Elements*; Wiley: New York, 1991; p 276.
(70) Stewart, R. F.; Jensen, L. H. *Acta Crystallogr.* **1967**, *23*, 1102.
(71) Henry, E. R.; Szabo, A. *J. Chem. Phys.* **1985**, *82*, 4753.
(72) Ishii, Y.; Terao, T.; Hayashi, S. *J. Chem. Phys.* **1997**, *107*, 2760.
(73) Parry, G. S. *Acta Crystallogr.* **1954**, *7*, 313.
(74) Ferenczy, G.; Harsanyi, L.; Rozsondai, B.; Hargittai, I. *J. Mol. Struct.* **1986**, *140*, 71.
(75) Marsh, R. E. *Acta Crystallogr.* **1958**, *11*, 654.
(76) Mattingly, S. M.; Vogt, F. G.; Gibson, J. M.; Mueller, K. T. "Determination of Molecular Geometry through Solid-State NMR: A Precision Analysis of the Intervector Angle of Three-Spin Systems," poster presented at the 43rd Rocky Mountain Conference on Analytical Chemistry, Denver, Colorado, Aug., 2001.
(77) Mattingly, S. M.; Vogt, F. G.; Gibson, J. M.; Mueller, K. T., manuscript in preparation.